Thermo-Physical Properties for Process Control

Brian J. Monaghan and Robert F. Brooks

National Physical Laboratory, Teddington, London, TW11-OLW, UK.

Thermo-physical properties have been shown to be important in a number of industrial processes. Unfortunately for a number of properties, there are scant data available and/or the data that are available are of dubious quality. In the Thermo-Physical Property Group at the National Physical Laboratory (NPL) we aim to develop measurement techniques capable of working in the difficult environments, that are typical of industrial processes. This paper represents current developments at NPL in our measurement techniques to measure the thermal diffusivity of liquid slags using a laser flash and insights into the copper smelting process using interfacial tension techniques.

Thermo-Physical Properties for Process Control

1. Introduction

Computer models that simulate industrial processes are increasingly used to reduce costs and improve productivity. The success of such models is highly dependent on the thermo-physical property data used in the simulation calculations. There are little data available for these models and the data that are available are often of questionable quality. This lack of reliable thermo-physical data is a major impediment to realising the full potential of current process modelling technology. Most of the thermo-physical data that are available for liquid oxide systems are contained in the Slag Atlas data compendium [1] published in 1995.

The fact that there are scant liquid oxide data and that the data often has large uncertainties associated with them is symptomatic of the difficulty experienced in handling liquid oxide systems. The principle difficulties are :

a. Experimentally liquid oxides are difficult to handle. They are often reactive with both the containment vessel and atmosphere. This causes problems with reproducibility of measurement as the oxide changes composition. This is critical in surface tension measurements were small changes in composition can have a large effect on the measurement.
b. Liquid oxide measurements are invariably high temperature measurements. Most traditional thermo-physical property measurement techniques were designed for ambient or near ambient temperatures. Modifying these methods for high temperatures often increases the uncertainty in the measurement.
c. Heat transfer in liquid oxides is complex, involving phonon (thermal diffusion) and photon (radiation) conduction. It is difficult separate the radiation component of heat conduction from the thermal diffusivity measurements.
d. Also at the high temperatures encountered when dealing with liquid oxides, it is difficult to obtain the thermal stability in order to avoid convective (mass) flow in a sample. This can lead to apparently high measured thermal diffusivities.

Currently in the Materials Centre of the National Physical Laboratory (NPL) studies are on-going into the thermal, transport, interfacial and thermodynamic properties of liquid oxide systems. This paper summarises the developments carried out on the NPL thermal diffusivity laser flash apparatus (LFA) and the maximum bubble pressure (MBP) for the measurement of surface tension and density of liquid oxide systems.

2. Thermal Diffusivity

2.1. Thermal Diffusivity Measurement by the LFA

Thermal diffusivity is defined as the rate of heat diffusion per unit time, as given in Eq. 1 [2]:

(1) $$a = \frac{l}{Cp.r}$$

where:
a is the thermal diffusivity ($m^2\ s^{-1}$)

λ is the thermal conductivity ($W\ m^{-1}K^{-1}$)
Cp is the specific heat capacity ($J\ kg^{-1}K^{-1}$)
ρ is the density ($kg\ m^{-3}$)

A typical laser flash thermal diffusivity measurement involves heating the front face of a disc-shaped sample of known thickness using a high intensity laser and monitoring the temperature rise on the back face. From the temperature rise the thermal diffusivity can be calculated. A furnace is used to heat the sample to the desired temperature.

There are numerous models available to calculate the thermal diffusivity from the temperature transient of a single layer sample [3-7]. Making a thermal diffusivity measurement of a slag material is more complex, because the liquid oxide is held in a measurement cell. The effects of this measurement cell on the measured temperature transient is not negligible. In this paper the Lee's [8,9] three layer model is used to account for the cell effects the details of which have been described in detail elsewhere[8,9].

In Lee's model the unknown thermal diffusivity of the liquid oxide can be determined if the thermal properties (thermal diffusivity, heat capacity and density) of the cell and the heat capacity and density of the liquid oxide are known. The thermo-physical property data used in the three layer model are given in Appendix A, Tables A1 to A6.

Although density values used may change with temperature, no allowance is made for changes in thickness of any layers with respect to expansion. All values used for thickness are that measured at room temperature.

2.2 Experimental

2.2.1 The Measurement Cell

The measurement cell comprised of an alumina cap, platinum lid, platinum crucible and an alumina crucible support, as pictured in Figure 1. The primary function of the alumina cap is to ensure that the platinum lid is seated on the platinum crucible and not floating on the liquid slag surface. This enables definition of the sample thickness, a critical parameter in the measurement of thermal diffusivity. .

2.2.2 Materials Preparation

The composition of oxides measured in this study are given in Table 1 and were measured by British Steel Teesside Works.

The oxide material was added to the measurement cell in powder form and melted prior to measurement. This required more than one filling-melting sequence to ensure the cell was full.
In melting, a compromise had to be made between heating to a temperature that ensured the slag material was fully molten but not so high that significant quantities would be lost to the gas phase. All melting and measurements were carried out in an argon atmosphere.

2.3. Results/ Discussion

The results of measurements made on samples ASE and ASK are shown in Figures 2 and 3. Unless otherwise stated all sample thickness were of the order of 1.5 mm. Also none of the measurements presented in Figures 2 and 3 have been corrected for a radiation contribution and are therefore referred to as effective thermal diffusivity (a_e) .

On inspection of Figure 2 it can be seen that the measurements are, within the scatter in the data, good agreement. Also the effective thermal diffusivity shows an increase with increasing temperature.

The ASK measurements shown in Figure 3, were measured at two different thicknesses and on a heating and cooling cycle. In general the data shows a similar trend with temperature to ASE and that measuring on the heating (h) and cooling (c) cycles had no effect on the effective thermal diffusivity. Also, it is apparent from the graph that increasing the thickness increases the effective thermal diffusivity. The increased thicknesses of the sample was obtained by inserting a platinum ring between the platinum cell lid and crucible.

It is clear from Figures 2 and 3 that the LFA apparatus can make measurements on slags ASE and ASK. What is not so clear is what these measurements represent. Most slag materials of industrial interest are either transparent or semi-transparent to the infra-red wavelengths and the laser light wavelength of 1.064 μm used in the LFA [1,10,11]. As a consequence of this the heat transfer through the sample has both a phonon (thermal diffusion) and photon (radiation) contribution as shown in Eq. 2.

(2) $$a_e = a + a_{rad}$$

where a_{rad} is a radiation term. The significance of this radiation term will be dependent on the difference in temperature between the adsorbing and emitting surfaces (i.e. platinum surfaces if the slag is transparent, platinum surfaces and the slag if semi-transparent), the absorption/emission coefficient of the slag and the effective penetration depth of the radiation [12]. It is a difficult parameter to calculate because:

a. there are very little absorption/emission data on slags and the data that does exist has usually been measured at ambient temperature [1].
b. The power of laser pulse is never measured. This makes calculation of the surface temperature differences difficult.

The matter is further complicated by the fact to solve for a_e using the three layer model data for the heat capacity and density of the slag are also required. These data are often not readily available or of poor quality and as a result may have to be modelled. Further increasing the uncertainty the measured thermal diffusivity.

Most approaches to the radiation problem have involved modelling the data on a grey body [11,13] or transparent body [10] assumption. According to authors [10] the grey body assumption is only required for slags containing FeO or TiO_2.

If radiation is a problem in our measured data, then the measured (effective) thermal diffusivities would be expected to increase with increasing temperature and increasing size [1,10,11,13]. Inspection of both Figures 2 and 3 are consistent with such trends. It is

therefore likely that the measured thermal diffusivities do have a radiation component associated with them.

As mentioned previously Waseda et al [10] stated that a transparent body approximation to radiation could be used for slags that contained no FeO or TiO_2. They also developed [10] a set of equations that could correct for the effect of radiation under such conditions.

Their approach was as follows: they assumed a value for thermal diffusivity of a liquid slag material of 0.004 x 10^{-4} m^2s^{-1}. Then they modelled the effect radiation would have on a thermal diffusivity measurement using the LFA by a finite difference method.

For an effective thermal diffusivity as defined in Eq. 3,

(3) $$a_e = c \cdot a$$

where c is the effect of radiation, they proposed the following Eq.'s for c, for 0.1, 0.2 and 0.3 mm thick samples respectively.

(4) $$c = 2.549 \times 10^{-7} \cdot T^2 - 4.504 \times 10^{-4} \cdot T + 1.244$$

(5) $$c = 6.986 \times 10^{-7} \cdot T^2 - 1.466 \times 10^{-3} \cdot T + 1.883$$

(6) $$c = 1.253 \times 10^{-6} \cdot T^2 - 2.675 \times 10^{-3} \cdot T + 2.606$$

These equations have been derived for sample sizes much smaller than the ones measured by NPL. In order to utilise this approach the constants in Eq.'s 4 to 6 were linearly regressed with respect to sample thickness to obtain Eq.'s 7 and 8 for thickness' 1.53 mm and 2.05 mm respectively.

(7) $$c = 7.372 \times 10^{-6} \cdot T^2 - 1.628 \times 10^{-2} \cdot T + 10.968$$

(8) $$c = 9.967 \times 10^{-6} \cdot T^2 - 2.206 \times 10^{-2} \cdot T + 14.510$$

This is not a rigorous approach as it is always questionable using relations outside the region that they were derived for.

Ignoring heat loss effects, if there is not a radiation component to a thermal diffusivity measurement by the LFA then the values obtained should be independent of sample thickness [12]. Also for highly structured materials (crystalline solids) the phonon contribution would be expected to show a negative dependency of thermal diffusivity with increasing temperature [12]. This is a result of distortion of the thermal energy waves by the vibration of the lattice atoms in a crystalline structure. This vibration increases with increasing temperature. It is not so clear how a liquid structure would behave. If it was highly polymerised perhaps it would follow similar behaviour to a solid lattice with increasing temperature i.e. the thermal conductivity would decrease. Also it can be expected that for polymerised melts, the higher the temperature, the smaller the chain length [1]. The smaller the chain length the larger the number of molecules and therefore boundaries between molecules. This increase in the

number of boundaries will have a greater resistance to heat flow. Such a process is analogous to grain boundary effects in metal alloys, were the thermal conductivity is inversely proportional to the number of grain boundaries [12].

To assess the validity of Eq.'s 7 and 8, the data shown in Figure 3 for the two different sample thickness would be recalculated using Eq.'s 3, 7 and 8. The results are shown in Figure 4 and compared with values obtained from the Slags Atlas [1] for a material of a similar composition to ASK. If the radiation component has been assessed correctly the thermal diffusivities should be independent of sample thickness i.e. reduce to one line. Also from the foregoing argument on conductivity with temperature it to be expected that the diffusivity would decrease with increasing temperature.

On inspection of Figure 4, it can be seen that the data still persist as two lines although they are closer than in Figure 3. In Figure 3 the difference in the diffusivities between the 1.53 mm to 2.06mm slag samples is approximately 100%, compared with 25 % for the corrected values shown in Figure 4. Also the curves do show a negative dependency of thermal diffusivity on increasing temperature. This would suggest that the radiation correction derived for the small sample size may have limited application at the thickness employed in this study. Also when comparing the values obtained with those of a similar slag composition [1], it can be seen, particularly for the smaller sample, that the agreement is reasonable.

From the data shown in Figure 4, it can be concluded that corrections for radiation can be made, but if the capability of LFA technique for measuring thermal diffusivities of slags is to be fully realised, then the effects of radiation for it's particular sample geometry have to be determined. Also the radiation correction used was for a transparent body approximation. This would not be appropriate for semi-transparent materials and other corrections would have to be determined. This would require data on the optical properties of the slag materials. At present these data either do not exist, are of poor quality or are available at unsuitable temperatures.

3. Surface Tension

3.1. Surface Tension Measurement by the MBP

Surface tension (γ), defined as the force resulting from the incomplete co-ordination of atoms residing at an interface between a solid or liquid with a gas, is an important parameter affecting flow and ware patterns in a number of industrial processes [12]. At NPL we have developed a MBP apparatus to measure the surface tension and density of liquid oxides.

An MBP measurement is made by measuring the pressure required to blow a bubble of gas at the end of a capillary submerged a known distance in the sample liquid. The surface tension can be calculated from Eq.9 [14].

$$g = \frac{rP_g}{2}\left\{1 - \frac{2}{3}\left(\frac{rrg}{P_g}\right) - \frac{1}{6}\left(\frac{rrg}{P_g}\right)^2\right\} \tag{9}$$

where P_r is defined by Eq. 10:

(10) $$P_g = P_m - rgh$$

and

r is the radius of the capillary (m)
ρ is the density of the liquid (kgm^{-3})
g is acceleration due to gravity (ms^{-2})
h is the depth of immersion of the capillary (m)
P_m is the maximum pressure measured (Pa)

Density can also be obtained from MBP measurements by blowing bubbles at two different depths using Eq. 11,

(11) $$r = \frac{(P_{m_2} - P_{m_1})}{g(h_2 - h_1)}$$

where the suffixes 1 and 2 denote measurements at two distinct depths.

3.2. Experimental

The apparatus consisted of an alumina environmental chamber enclosed in a resistance furnace, with an alumina capillary (3mm internal diameter) inserted through an o-ring seal at the top of the chamber. The samples were held in an alumina or molybdenum crucible. The depth of immersion was measured relative to the liquid surface by a vernier calliper attached to the capillary lifting mechanism. The surface of the liquid oxide was detected by an increase in the gas pressure inside the capillary. On detection the vernier calliper was zeroed and depths measured directly from the calliper thereafter. The calliper had a resolution of 0.01mm. This was the principle error in the detection of the surface of the liquid oxide. The formation of argon bubbles were controlled by (fine) needle valves to obtain a bubble rate of approximately 6 bubbles per minute. Pressure was measured using pressure transducers, the output of which was read by digital voltmeter and logged to a PC.

The positioning of the capillary in the crucible is critical if end effects resulting from bubble interactions with the wall and the bottom of the crucible are to be avoided.

3.2.1. Materials Preparation

Measurements were made on a pre-fused decarburised mould flux (PMF) and a copper blast furnace slag (CBFS), the compositions of which are given in Table 2. The analysis of these materials came from the material suppliers, Carboox of Brazil and IMI Refiners of the UK, receptively. The Fe composition given in Table 2 for slag CBFS is primarily oxide. The samples were heated to a maximum temperature, measured, and then cooled for subsequent measurements.

The PMF was chosen as a relatively inert liquid oxide enabling testing of the measurement system. The crucible material used for PMF was molybdenum. The powdered sample was pre-melted in an induction furnace prior to measurement in the MBP apparatus. This melting was repeated until the crucible contained approximately 50 mm depth of oxide. Such a depth enabled measurements to be made at 3 or 4 depths, approximately 10 mm apart.

CBFS was a more reactive slag, and due to the high metal/iron oxide content, could not be melted into a molybdenum crucible. Therefore an alumina crucible was used. The high reactivity also meant that the sample could only be melted in-situ in the MBP apparatus. This limited the amount of material available for measurement, providing only enough to allow two depths (10 and 20mm) at each temperature. Also, to minimise the risk of damage to the MBP apparatus measurements were only made over a limited temperature range. Measurements of the viscosity of this material had already been attempted at higher temperatures in the NPL rotating bob viscometer resulting in considerable damage to the equipment.

3.3. Results/ Discussion

Results for PMF and CBFS are given in Figures 5 and 6 respectively. The different data points at a given temperature represent different measurements depths. In Figure 5, it can be seen that the surface tension values obtained are, within the scatter of the data, independent of measurement depth or temperature. The surface tension and density values for PMF in Figure 5 are consistent with values given in the Slag Atlas [1] for materials of similar composition.

In Figure 6, the surface tension data from the CBFS measurements, are with the exception of the highest temperature measurements, dependent on measurement depth. The density of the slag at this high temperature (1375°C) was 3389 kgm^{-3}. At temperatures lower than 1375°C, the pressures needed to generate the bubbles at the 20 mm depths were very much greater than the 10mm, resulting in the different (high) values of surface tension. Also at the lower depth at ~1305°C the capillary showed signs of blocking and no bubbles could be produced.

The difference in the behaviour of the PMF and CBFS is stark. The PMF measurements were independent of depth, as expected, whereas the measurements of the CBFS were depth dependent. This anomalous behaviour was in part expected. The PMF material was chosen as benign slag that would be fully liquid and single phase over the temperature range measured. Thus enabling testing of the MBP apparatus's performance. The scatter in the PMF data are considered representative for such a benign material. In contrast the CBFS slag was known to be extremely reactive and therefore a challenging materials to perform measurements on.

CBFS, is a high iron oxide slag and unlikely to be stable in the relatively reducing furnace atmosphere of argon. The iron oxide would partially reduce to metallic iron under such conditions. Also, given the composition of CBFS, it is likely to be reacting with both the crucible and the capillary taking more Al_2O_3 into solution. Further uncertainty over the composition of the CBFS slag arises from the fact that it was unclear whether the Zn and Cu were in their metallic or oxide form in the slag. In summary, the slag composition is changing with time and may be two or three phase. If the slag was more than one phase it may stratify with composition as a result of the density differences of the different phases or reaction rates.

The cooled crucible containing the CBFS sample used in the measurement was sectioned and visually inspected for stratification. A photograph showing the sectioned crucible is given in Figure 7. The sample was found to contain small metallic particulates throughout the melt. Also the colour change of the slag from top to bottom indicated that there was composition stratification. Figure 7 also shows some evidence of reaction between the slag and the Al_2O_3

crucible, indicated by the colour change of the Al_2O_3 close to the Al_2O_3-slag interface. Given the conformation of the variable composition and mixed phases of slag CBFS, it is no surprise that the surface tension measurements were anomalous.

In an attempt to understand the behaviour of the sample effects of changing slag and gas composition on the liquidus temperature were made using the NPL MTDATA thermodynamic software [15]. The MTDATA software uses internationally validated thermodynamic databases [15]. For an initial slag composition based on the composition of CBFS in Table 2 without Zn and Cu, calculations of the liquidus temperature of the slag were made for a range of pO_2's. The reason for not using the full CBFS composition as the base composition was that the thermodynamic data base did not include all the required data.

Liquidus temperatures were then calculated for a similar slag over the same pO_2 range but with an increasing Al_2O_3 content of 10 and 20 % respectively, to mimic alumina pickup from the crucible material. On the assumptions of ideal behaviour for Cu system interactions with MgO and Al_2O_3 and Zn system interactions with MgO, a further set of liquidus calculations where made using the composition of CBFS given in Table 2. The results of these calculations are given in Figure 8.

The pO_2's in the argon atmosphere of the MBP furnace will be of the order of 10^{-5} and 10^{-6}. Over this pO_2 range the liquidus temperature was relatively insensitive to increasing the Al_2O_3 from base to 20%. Also, over this pO_2 range the addition of Cu and Zn has little effect on the liquidus temperature. The largest liquidus temperature change being from 1350°C to 1370°C. These liquidus temperatures were greater than all but the highest temperatures for the surface tension measurements in Figure 6. Therefore, if these liquidus temperatures are correct the slag must have been two phase, both liquid and solid, during all but the highest temperatures for the surface tension measurements. This is likely to explain the disparity between the surface tension measurements at different depths. At the lower depths, probably due to some cementation, the bubble was encountering a different slag composition. This slag would have been two phase. The two phase slag at the bottom of the crucible would have a higher effective viscosity, making the displacement of the liquid by the bubble more difficult. A higher pressure is then required to form the bubble. The same effect can be observed when the bubble approaches a solid surface, such as the bottom of the crucible. Higher pressure is needed to displace the liquid resulting in a higher apparent surface tension.

4. Conclusions

a. The LFA is capable of measuring effective thermal diffusivities but more research into the optical properties of the slag is required before definitive values of thermal diffusivity can be obtained by this method.

b. Heat capacity and density data are required for the slag to calculate the thermal diffusivities from the three layer model. There is a paucity of such data for liquid slags. If there is a requirement for thermal diffusivity measurements of slags, then issues relating to the limited data sets available for heat capacity and density of slags will have to be addressed.

d. The effective thermal diffusivities of the mould power ASE and CaO-Al_2O_3-SiO_2 slag ASK are of the order 0.005×10^{-4} m^2s^{-1}.

e. The surface tension and density of PMF is 320mNm^{-1} and 2600kgm^{-3} over the temperature range of 1200 to 1400°C.

f. The MBP results, and MTDATA calculations, show that the liquid is homogeneous at temperatures above 1370 °C and that the surface tension of CBFS is approximately 550mNm^{-1}.

Acknowledgements

This work was carried out as part of the Materials Measurement Programme of the Department of Trade and Industry. Thanks are due to Prof. K. C. Mills of Imperial College London, UK, Prof. Y. Waseda of Tohoku University, Sendai, Japan, Netzsch in Selb, Germany, Mr M. Doe of IMI Refiners, Walsall, UK and Carboox of Brazil for helpful discussion, advice and materials during the course of this study.

References

1. Slag Atlas, 2nd Edition: Verlag Stahleisen GmBH, Dusseldorf, Germany, 1995.
2. Carslaw, H.S. and Jaeger, J.C.: Conduction of Heat in Solids, Oxford University Press, Oxford, UK, 1959.
3. Parker, J. and Butler, A.: J. Appl. Phys., Vol. 32, 1961, p1679.
4. Taylor, R.E. and Clark, L.M.: High Temp. High Pres., Vol. 6, 1974,p65.
5. Cowan, R.D.: J. Appl. Phys., Vol. 34, 1963, p926.
6. Clark, L.M. and Taylor, R.E.: J. Appl. Phys., Vol. 46, 1975, p714.
7. Dusza, L.; High Temp. High Press., Vol. 27/28, 1995/1996, p467.
8. Netzsch Operating Instructions, Part A- Theoretical background, LFA 427, Operating Instructions, 09.93, Selb, Germany.
9. Lee, H.J.: Ph.D. Thesis, Purdue University, USA, 1967.
10. Waseda, Y., Masuda, M., Watanabe, K., Shibata, H., Ohta, H. and Nakajima, K.: High Temp. Mat. Proc., Vol. 13, 1994, p267.
11. Srinivasen, N.S., Xiao, X.G. and Seetharaman, S.: J. Appl. Phys., Vol. 75, 1994, p2325.
12. Poirier, D. R. and Geiger, G.H.: Transport Phenomena in Materials Processing, TMS, Warrendale, PA, USA, 1994.
13. Maeda, Y., Sagura, H., Tye, R,, Masuda, M., Ohta, H. and Waseda, Y.: Int. J. Thermo. Phys., Vol. 17, 1996, p253.
14. Garcia-Cordonvilla, C., Louis, E. and Pamies, A.: J Materials Science, Vol. 21, 1986, p2287.
15. Davies, R. H., Dinsdale, A.T., Gisby, J.A., Hodson, S.M., and Ball R.G. J.: Proc. Conf. Applications Thermodynamics on the Synthesis and Processing of Materials, ASM/TMS, Rosemont, IL, USA, 1994.

Figure 1. Picture of slag cell (lid and crucible), holder and cap.

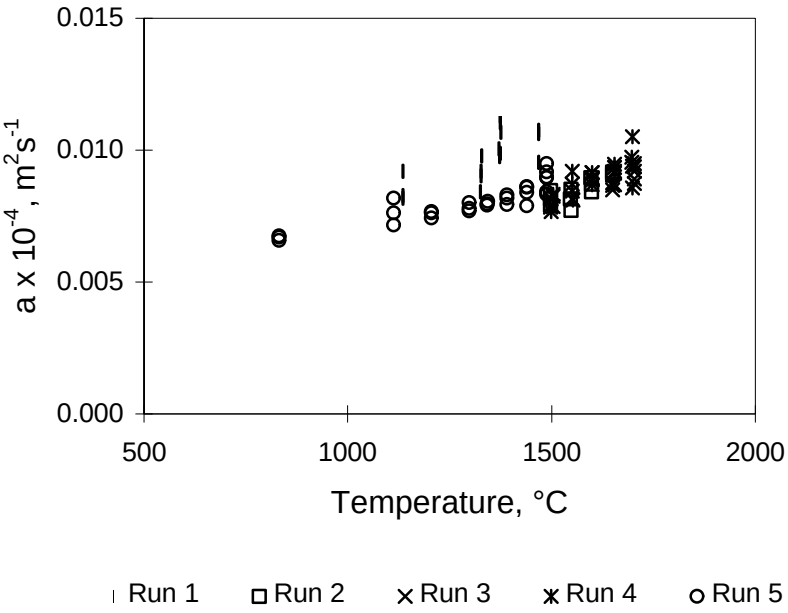

Figure 2. Effective thermal diffusivity (a_e) measurements made by a number of laboratories on slag ASE.

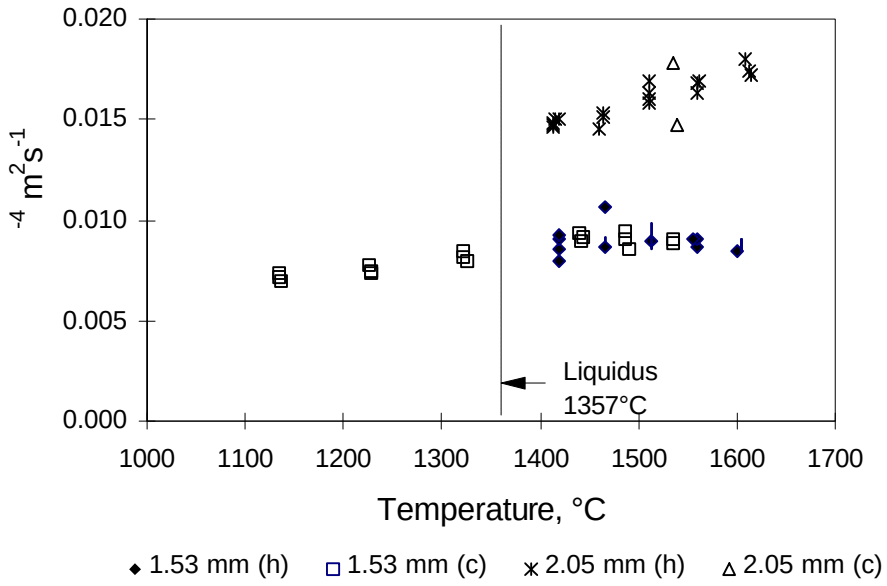

Figure 3. Effective thermal diffusivity (a_e) measurements of slag ASK at two different sample thickness.

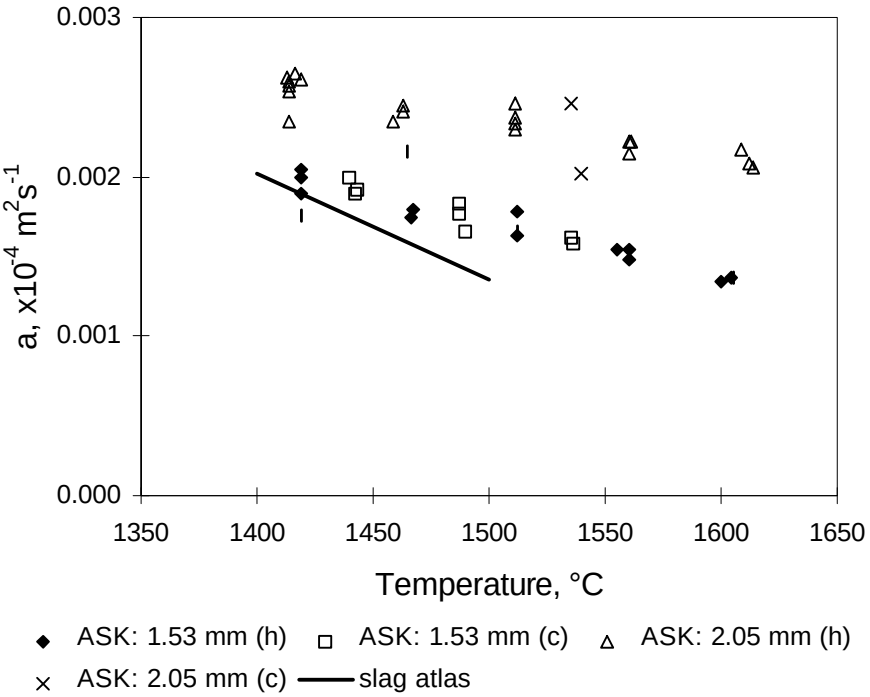

Figure 4. ASK thermal diffusivity measurements corrected for radiation contribution. The slag atlas [1] composition in weight % is 25 % CaO, 15% Al_2O_3, and 60% SiO_2.

Figure 5. Surface tension and density measurements for sample PMF.

Figure 6. Surface tension and density measurements for sample CBFS.

Figure 7. Photograph of the sectioned alumina crucible plus CBFS sample.

Figure 8. MTDATA [15] liquidus calculations for slag compositions based on CBFS at different pO_2's.

Table 1. Slag compositions in weight %.

Material	Fe (total)	CaO	SiO_2	Al_2O_3	S
ASE1	1.06	34.92	38.44	6.72	0.092
(Decarburised mould flux)	Na_2O	F	other	-	-
	12.25	6.66	balance	-	-
Material	CaO	SiO_2	Al_2O_3	other	-
ASK	15.52	64.51	15.05	balance	-

Table 2. Slag compositions in weight %.

	SiO_2	Al_2O_3	CaO	MgO	Na_2O	F	Fe	Zn	Cu
PMF	37.9	6.2	35.5	-	9.3	6.4	-	-	-
CBFS	25.7	12.9	-	3.1	-	-	32.7	4.6	1.5

Appendix A

Table A1. Heat capacity values of the platinum cell.

Temperature, °C	Heat Capacity, $Jg^{-1}K^{-1}$
20	0.1420
100	0.1460
200	0.1490
300	0.1530
400	0.1570
500	0.1600
600	0.1630
700	0.1660
800	0.1690
900	0.1730
1000	0.1760
1100	0.1790
1200	0.1820
1300	0.1850
1400	0.1880
1500	0.1900
1600	0.1940
1700	0.1970
I740	0.1980

Table A2. Density values of the platinum cell.

Temperature, °C	Density, gcm^{-3}
20	20.000
100	19.956
200	19.900
300	19.842
400	19.783
500	19.722
600	19.660
700	19.597
800	19.532
900	19.464
1000	19.395
1100	19.320
1200	19.252
1300	19.177
1400	19.099
1500	19.017
1600	18.933
1700	18.850
1800	18.767

Table A3. Thermal diffusivity values of the platinum cell.

Temperature, °C	Thermal Diffusivity, cm^2s
28	0.1371
195	0.1630
392	0.1840
588	0.1973
794	0.2075
996	0.2175
1190	0.2221
1405	0.2290
1600	0.2338
1700	0.2358
1800	0.2373

Table A4. Heat capacity values of ASK

Temperature, °C	Heat Capacity, $Jg^{-1}K^{-1}$
1000	1.4443
1100	1.4443
1200	1.4443
1300	1.4443
1356	1.4443
1357	1.4443
1400	1.4443
1500	1.4443
1600	1.4443
1700	1.4443

Table A5. Density values of ASK

Temperature, °C	Density, gcm^{-3}
1000	2.6386
1100	2.6111
1200	2.5842
1300	2.5578
1356	2.5433
1357	2.543
1400	2.532
1500	2.5067
1600	2.4819
1700	2.4575

Table A6. Density and specific heat values of ASE

Temperature, °C	Density, gcm^{-3}	Heat Capacity, $Jg^{-1}K^{-1}$
All temperatures	2.7	1.35